DOI 10.1007/s10778-019-00961-3
International Applied Mechanics, Vol. 55, No. 4, July, 2019

TECHNIQUE OF ALLOWING FOR PLASTIC STRAINS UNDER UNLOADING IN THERMOPLASTICITY PROBLEMS FOR AXISYMMETRIC BODIES

V. G. Savchenko and M. E. Babeshko

The nonaxisymmetric elastoplastic stress–strain state of bodies of revolution under nonisothermal combined loading is analyzed with allowance for secondary plastic strains. The study is based on the use of the constitutive equations of the theory of small-curvature processes and finite-element method. The model of elastic unloading of a material with perfect Bauschinger effect and isotropic hardening is employed. Numerical examples illustrate how the choice of an unloading model affects the results obtained.

Keywords: thermoplasticity, bodies of revolution, nonaxisymmetric stress–strain state, isotropic material, elastic unloading, perfect Bauschinger effect, isotropic hardening, secondary plastic strain

Introduction. The intensive development of modern mechanical engineering and the release of competitive products are impossible without fundamentally new ideas, mathematical modeling of the processes taking place in the structural elements, and the subsequent computational experiment. In this case, the original object is replaced by its mathematical model which is then analyzed and tested with the help of computational-logical algorithms. One of the factors contributing to solving such problems is the development of techniques capable of analyzing in detail the temperature fields and elastoplastic stress–strain state (SSS) of structures of wide class making the most complete allowance for features of their deformation under the operation and extreme conditions. Such an approach makes it possible to ensure necessary performances and high service reliability of the product at scarce funds for complex and expensive tests.

A feature of the deformation of structural members subject to intensive external heating is that the compressive stresses in the surface layers decrease with increasing temperature and turn into tensile when the plastic strains reverse sign. This is because, despite the temperature increase, the heating of the bulk of the element decreases the temperature gradient in the surface layers.

There are many developments [2–8, 15, etc.] that allow quasistatic elastic or elastoplastic analysis of nonuniformly heated structural members. However, the classes of the problem being solved are limited by various simplifying assumptions allowing describing only partial cases of the deformation process of the structural member under consideration. Some of these studies assume only elastic behavior of the member material over the whole range of stress variation, while others adopt the physically nonlinear stress–strain relationship with the unloading being neglected. It is often assumed that simple processes of deformation occur, accompanied by elastic unloading only. In reality, however, under intensive heating and mechanical loading, the deformation occurs along small-curvature paths [3, 10, 11, 20, 21] accompanied by secondary plastic strains under unloading. All these studies use modified relations of the theory of small-curvature processes [6, 18] and conventional relations of the theory of simple processes based on the Prandtl–Reuss theory [16, 17] and the Hencky theory [14], respectively.

The studies on small-curvature processes are mainly concerned with the SSS of shells of revolution under repeated thermomechanical loading with allowance for secondary plastic strains [9–12, etc.]. In what follows, we will consider a technique of numerical analysis of structural members in the form of bodies of revolution. The technique takes into account the

S. P. Timoshenko Institute of Mechanics, National Academy of Sciences of Ukraine, 3 Nesterova St., Kyiv, Ukraine 03057; e-mail: plast@inmech.kiev.ua. Translated from Prikladnaya Mekhanika, Vol. 55, No. 4, pp. 101–112, July–August 2019. Original article submitted April 26, 2018.

occurrence and variation in the plastic strains under unloading and nonisothermal loading. The results obtained with this technique in the case of variable nonisothermal loading assuming different material behavior under unloading (elastic unloading, isotropic hardening or perfect Bauschinger effect) will be analyzed. We will also study the plastic zones that occur during deformation.

1. Problem Statement. Governing Equations. Let us consider a compound (layered) body of revolution with isotropic and orthotropic elements under nonisothermal loading by volume, $\vec{K}(K_z, K_r, K_\varphi)$, and surface, $\vec{t}_n(t_{nz}, t_{nr}, t_\varphi)$, forces in given heating conditions. The body is described in the cylindrical coordinate system z, r, φ. It is assumed that the body temperature is T_0 at the initial instant t_0. The body is discretely homogeneous and composed of bodies of revolution with the common axis of revolution. The components of the body were joined at temperature T_0 without tension so that they are in perfect mechanical and thermal contact. The body is loaded so that the problem can be considered quasistatic.

In solving a thermoviscoplasticity problem, the process of loading and heating is divided into stages in such a way that a broken curve accurately matches the deformation path, while the time instants separating these stages are as close as possible to the instants at which the components change over from active loading to unloading and vice versa. To determine the thermoviscoplastic SSS of the body of revolution, it is necessary to sequentially solve the nonstationary thermal conduction problem to determine the temperature T under given conditions of heat exchange with environment and the thermoviscoplasticity problem to determine the displacements u_i, strains ε_{ij}, and stresses σ_{ij} $(i, j = z, r, \varphi)$ at fixed time instants under given loading and boundary conditions.

In studying the temperature and stress–strain state of the body, we will use the following variational equations:

heat conduction equation

$$\int_V \left[c\rho \frac{\partial T}{\partial t} \delta T - q_z \delta\left(\frac{\partial T}{\partial z}\right) - q_r \left(\frac{\partial T}{\partial r}\right) - q_\varphi \left(\frac{1\partial T}{r\partial \varphi}\right)\right] dV + \int_\Sigma \alpha(T-\theta)\delta T d\Sigma = 0 \tag{1}$$

and Lagrange equation

$$\int_V (\sigma_{ij}\delta\varepsilon_{ij} - K_i \delta u_i) dV - \int_{\Sigma_t} t_{ni}\delta u_i d\Sigma = 0 \quad (i, j = z, r, \varphi), \tag{2}$$

where V is the volume of the body of revolution bounded by the surface Σ; Σ_t is the part of the surface Σ on which the components of the surface load $\vec{t}_n$ act; c and ρ are the mass specific heat and the density of the body, respectively; α is the convective heat-transfer factor between the body and the environment of temperature θ; t is the current time of heating and loading; q_z, q_r, q_φ are the reduced heat fluxes in the respective directions:

$$q_z = -\left(\lambda_{zz}\frac{\partial T}{\partial z} + \lambda_{zr}\frac{\partial T}{\partial r} + \lambda_{z\varphi}\frac{1}{r}\frac{\partial T}{\partial \varphi}\right),$$

$$q_r = -\left(\lambda_{zr}\frac{\partial T}{\partial z} + \lambda_{rr}\frac{\partial T}{\partial r} + \lambda_{r\varphi}\frac{1}{r}\frac{\partial T}{\partial \varphi}\right),$$

$$q_\varphi = -\left(\lambda_{z\varphi}\frac{\partial T}{\partial z} + \lambda_{r\varphi}\frac{\partial T}{\partial r} + \lambda_{\varphi\varphi}\frac{1}{r}\frac{\partial T}{\partial \varphi}\right), \tag{3}$$

where λ_{ij} are the components of the heat conductivity tensor.

The constitutive equations relate the stresses σ_{ij} and the strains ε_{ij} relations; their coefficients depend on the type of material, equations of state, linearization method, etc. The strain tensor is represented as the tensor sum of elastic, plastic, and creep strains. At each loading stage, the thermoviscoplasticity problem is solved by the method of successive approximations. In this case, the constitutive equations become [19]:

$$\sigma_{ij} = A_{ijmn}\varepsilon_{mn} - \sigma^*_{ij} \quad (m, n = z, r, \varphi), \tag{4}$$

where

$$A_{ijmn} = A_{jimn} = A_{ijnm} = A_{mnij}. \tag{5}$$

The coefficients A_{ijmn} appearing in (4) and (5) are different for each type of material and depend on the plasticity and creep theories used. The terms σ_{ij}^* allow for the thermal strains, deviation of the material from elastic behavior, temperature dependence of stress–strain diagrams, type of anisotropy, the method used to linearized the constitutive equations, etc. To linearize the constitutive equations, we will use the methods of successive linear approximations, where the problem at each approximation is reduced to a linear elasticity problem with additional term σ_{ij}^*. These terms are determined from the previous approximation. The expressions for A_{ijmn} and σ_{ij}^* (4), (5) for isotropic material, cylindrically orthotropic, and linearly orthotropic materials are presented in [3, 19]. In describing the inelastic deformation of isotropic materials at each loading step, we will use the relations between σ_{ij} and ε_{ij} of the theory of small-curvature processes linearized by the additional stress method [4]. In this case, the stresses σ_{ij} and strains ε_{ij} in any element of the isotropic body are related by Hooke's law with additional terms allowing for the thermal strain, deviation of the material from elastic behavior, and the temperature dependence of elastic characteristics:

$$\sigma_{zz} = (2G_0 + \lambda_0)\varepsilon_{zz} + \lambda_0(\varepsilon_{rr} + \varepsilon_{\varphi\varphi}) - \sigma_{zz}^*,$$

$$\sigma_{zr} = 2G_0\varepsilon_{zr} - \sigma_{zr}^* \quad (z, r, \varphi), \tag{6}$$

where

$$\sigma_{ij}^* = 2G_0\omega\varepsilon_{ij} + 2G\varepsilon_{ij}^n + [(K_0\omega_1 + 2G_0\omega)\varepsilon_0 + K\varepsilon_T]\delta_{ij}, \tag{7}$$

$$\omega = 1 - \frac{G}{G_0}, \quad \omega_1 = 1 - \frac{K}{K_0}, \quad \lambda_0 = \frac{K_0 - 2G_0}{3}, \quad K = \frac{2G(1+\nu)}{1-2\nu},$$

$$\varepsilon_0 = (\varepsilon_{zz} + \varepsilon_{rr} + \varepsilon_{\varphi\varphi})/3, \quad \varepsilon_T = \alpha_T(T - T_0), \tag{8}$$

where G_0, G and K_0, K are the shear and bulk moduli at the initial and current temperatures, respectively; ν is Poisson's ratio; ε_{ij}^n are the inelastic strain components accumulated to the end of the mth loading step, which are equal to the inelastic components of the strain deviator e_{ij}^n due to plastic incompressibility,

$$(e_{ij}^n)_m = \sum_{k=1}^{m} \Delta_k e_{ij}^n = \sum_{k=1}^{m} \left\langle \frac{s_{ij}}{S} \right\rangle_k \Delta_k \Gamma_n. \tag{9}$$

The increments $\Delta_k\Gamma_n$ over the kth loading step are determined by the method of successive approximations in solving the boundary-value problem. Here $\Delta_k\Gamma_n = \Delta_k\Gamma_p + \Delta_k\Gamma_c$, and it is assumed that at the beginning of the mth loading step, the values of the instantaneous inelastic stain $\Gamma_n^{m-1} = \sum_{k=1}^{m-1}\Delta_k\Gamma_n$ obtained at the end of the previous $(m-1)$th step are known.

In the general case, the intensity of tangential stresses $S = (s_{ij}s_{ij}/2)^{1/2}$ is a functional of the intensity of shear strains $\Gamma = (e_{ij}e_{ij}/2)^{1/2}$, intensity of inelastic shear strains $\Gamma_n^m = \sum_{k=1}^{m}\Delta_k\Gamma_n$ accumulated over m steps, temperature T, and time t [5]:

$$S = F(\Gamma, \Gamma_n, T, t). \tag{10}$$

The functional is specified using the tensile and compressive stress–strain diagrams after achievement of a fixed value of the plastic strain of cylindrical specimens obtained at different temperatures and loading rates. These tests use used to plot a set of instantaneous thermomechanical surfaces $S = F^*(\Gamma^*, \Gamma_p^*, T)$ for different temperatures under loading and unloading allowing for the achieved plastic strains. The loading rate is allowed for by plotting the associated creep diagrams

$\varepsilon_c = \varepsilon_c(\sigma, T, t)$. The transformation from the uniaxial SSS to the intensity of tangential stresses S and to the intensity of shear strains Γ can be performed using the formulas

$$S = \frac{\sigma}{\sqrt{3}}, \quad \Gamma = \frac{1+\nu^*}{\sqrt{3}}\varepsilon, \quad \Gamma_p = \frac{\sqrt{3}}{2}\varepsilon_p, \quad \nu^* = \frac{1}{2} - \frac{1-2\nu}{4G(1+\nu)}\frac{\sigma}{\varepsilon}. \tag{11}$$

In what follows, we will consider deformation processes without creep strains. In this case, the functional dependence (10) transforms into a function representing the set of instantaneous thermomechanical surfaces $S = F^*(\Gamma, \Gamma_p, T)$. Some experimental results on material behavior under repeated deformation for cylindrical Kh18N10T steel specimens are outlined in the paper [9], which presents the dependences of the elastic moduli and Poisson's ratio under unloading on the preliminary plastic strain, evaluates the direct Bauschinger effect depending on the plastic strain, and presents some diagrams of repeated deformation after preliminary deforming. Test show that the dependences $S - \Gamma - \Gamma_p - T$ can be specified using only the stress–strain diagrams (σ vs ε) of active loading of the specimens and the compressive yield stress σ_T^- after preliminary tension depending on the accumulated plastic strain ε_p at different temperatures (or after preliminary compression followed by tension). For many materials, the compressive yield stress appears lower by 10–15% than the tensile yield stress. This difference is mainly attributed to the preliminary plastic deformation.

The deformation process can be divided into two stages: active loading with increasing plastic strains and unloading with either constant (elastic unloading) or decreasing plastic strains.

In active deformation from the natural stress state, $\Delta_k \Gamma_p$ is determined from the initial diagrams $S = \Phi(\Gamma, T)$. A technique for determining increments of the intensity of inelastic shear strains from these diagrams is detailed in [3, 19]. When a body element is unloaded and loaded by a load of opposite sign in the range of plastic strains, the function $S = \Phi(\Gamma, T)$ can be represented as

$$S = S_T^+ - S_T^- - \Phi\left(\Gamma^* + \frac{S_T^+ - S_T^-}{2G(T)}, T\right), \tag{12}$$

where $S_T = S_T^+ = \sigma_T^+ / \sqrt{3}$ is the intensity of tangential stresses corresponding to the yield stress in uniaxial tension; $S_T^- = \sigma_T^- / \sqrt{3}$ is the intensity of tangential stresses corresponding to the yield stress in compression after preliminary tension to the plastic strain $\varepsilon_p^{(1)}$ at the instant of unloading $\Gamma_p^{(1)} = \sqrt{3}\varepsilon_p^{(1)} / 2$; $\Gamma^* = [(\varepsilon_{ij} - \varepsilon_{ij}^{1(p)})(\varepsilon_{ij} - \varepsilon_{ij}^{1(p)} / 2)]^{1/2}$ is the intensity of shear strains; $\varepsilon_{ij}^{1(p)}$ are the components of plastic strains at the beginning of unloading.

In many cases, the stress state of structural members made of specific materials is studied in the absence of test data on the dependence of the yield stresses on the plastic strain. To describe the unloading and the loading of a body element by a load of reverse sign in such cases, it is necessary to assume either elastic unloading, or isotropic hardening, or perfect Bauschinger effect, etc.

In the case of elastic unloading, we have

$$S = 2G(\Gamma_p^{(1)}, T)(\Gamma - \Gamma_p^{(1)}). \tag{13}$$

In the case of isotropic hardening under unloading and reverse-sign loading, we have

$$S = S_T - S^{(1)} - \Phi\left(\Gamma^* + \frac{S_T - S^{(1)}}{2G(T)}, T\right), \tag{14}$$

where $S^{(1)}$ is the intensity of tangential stresses corresponding to the plastic strain (9) at the instant of unloading.

If the material under unloading and reverse-sign loading obeys the perfect Bauschinger effect, then

$$S = S^{(1)} - S_T - \Phi\left(\Gamma^* + \frac{S^{(1)} - S_T}{2G(T)}, T\right). \tag{15}$$

As follows from [9], these models of material behavior cover the range that includes the unloading and repeated loading curves of many materials. This makes it possible to perform a number of calculations to estimate SSS that complies with real curves allowing for unloading and reverse-sign loading.

In solving spatial problems for bodies of revolution, we will use the semi-analytical finite-element method [3, 6, 13, etc.], which expands the candidate solution into series:

$$T(z,r,\varphi,t)=\sum_{m=0}^{\infty}\overline{T}_m(z,r,t)\cos m\varphi+\sum_{m=1}^{\infty}\overline{\overline{T}}_m(z,r,t)\sin m\varphi, \tag{16}$$

$$u_z(z,r,\varphi,t)=\sum_{m=0}^{\infty}\overline{u}_z^{(m)}(z,r,t)\cos m\varphi+\sum_{m=1}^{\infty}\overline{\overline{u}}_z^{(m)}(z,r,t)\sin m\varphi \quad (z,r),$$

$$u_\varphi(z,r,\varphi,t)=\sum_{m=1}^{\infty}\overline{u}_\varphi^{(m)}(z,r,t)\sin m\varphi+\sum_{m=0}^{\infty}\overline{\overline{u}}_\varphi^{(m)}(z,r,t)\cos m\varphi, \tag{17}$$

where the coefficients are determined using the appropriate variational equations (1)–(3) and the finite elements in the meridional section of the body.

With such an approach, the problem for bodies of revolution can be reduced to a number of two-dimensional variational problems for the unknown coefficients in series (16), (17). To this end, in solving the heat conduction problem, it is necessary to represent the coefficients λ_{ij} in (1) in the form $\lambda_{ij}=\lambda_{ij}^0(1-\omega_{ij}^T)$ and to assume that at some fixed instant of time, the heat-transfer factor α, the environment temperature θ, reduced heat fluxes q_z, q_r, q_φ, and the product $c\rho$ are known constant coordinate functions. We will use triangular finite elements with linearly varying coefficients $\overline{T}_m$ and $\overline{\overline{T}}_m$ in the meridional section. Considering the coefficients $\overline{T}_m$ at the vertices (i,j,k) of the elements with the side ij coinciding with the body surface in the case where the thermal conduction problem is solved with an explicit difference scheme, we arrive at the recurrent formulas

$$\overline{T}_{mi}(t+\Delta t)=\overline{T}_{mi}(t)+\frac{\Delta t}{\sum_{q=1}^{M}\langle c\rho\rangle_q H_i^{(q)}}\sum_{q=1}^{M}\Big[A_{ij}\overline{\theta}_{mi}(t+\Delta t)+B_{ij}\overline{\theta}_{mj}(t+\Delta t)$$

$$-(D_{ii}+m^2N_{ii}+A_{ij})\overline{T}_{mi}(t)-(D_{ij}+m^2N_{ij}+B_{ij})\overline{T}_{mj}(t)-(D_{ik}+m^2N_{ik})\overline{T}_{mk}(t)$$

$$+L_i(\overline{q}_z^{*(m)}(t)-\overline{\overline{q}}_{z\varphi}^{*(m)}(t))_i+P_i(\overline{q}_r^{*(m)}(t)-\overline{\overline{q}}_{r\varphi}^{*(m)}(t))_i-mR_i\overline{q}_\varphi^{*(m)}(t)\Big]_q, \quad (i=1,2,\ldots,N), \tag{18}$$

which allow finding the values of the coefficients $\overline{T}_m$ at the instant $t+\Delta t$ from their values at the instant t. If the problem is solved using an implicit difference scheme, we obtain the system of equations

$$\sum_{q=1}^{M}\Big[(D_{ii}+m^2N_{ii}+\frac{1}{\Delta t}\langle c\rho\rangle H_i+A_{ij})\overline{T}_{mi}(t+\Delta t)+(D_{ij}+m^2N_{ij}+B_{ij})\overline{T}_{mj}(t+\Delta t)$$

$$+(D_{ik}+m^2N_{ik})\overline{T}_{mk}(t+\Delta t)\Big]_q$$

$$=\sum_{q=1}^{M}\Big[\frac{1}{\Delta t}\langle c\rho\rangle H_i\overline{T}_{mi}(t)+A_{ij}\overline{\theta}_{mi}(t+\Delta t)+B_{ij}\overline{\theta}_{mj}(t+\Delta t)$$

$$+L_i(\overline{q}_z^{*(m)}(t)-\overline{\overline{q}}_{z\varphi}^{*(m)}(t))+P_i(\overline{q}_r^{*(m)}(t)-\overline{\overline{q}}_{r\varphi}^{*(m)}(t))-mR_i\overline{q}_\varphi^{*(m)}(t)\Big]_q \quad (i=1,2\ldots,N). \tag{19}$$

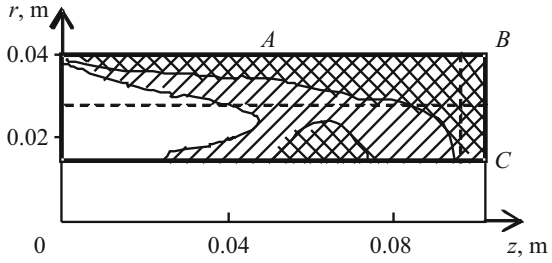

Fig. 1

Here m is the harmonic number; N is the number of nodal points; M is the number of triangular elements in the meridional section; q is the triangular element number; $\overline{\theta}_{mi}$, $\overline{\overline{\theta}}_{mi}$, $\overline{q}_i^{*(m)}$, and $\overline{\overline{q}}_{ij}^{*(m)}$ are the coefficients of expansion of the environment temperature and reduced heat fluxes (3) into trigonometric series, similar to (16), at the appropriate points of the triangular being considered. Similarly, using the approach described in detail in [3, 4, 6], we obtain the following system of $3N$ linear algebraic equations for each harmonic for the determination of the coefficients $\overline{u}_\alpha^{(m)}$ and $\overline{\overline{u}}_\alpha^{(m)}$ $(\alpha = z, r, \varphi)$ at the vertices (i, j, k) of the triangular elements q of the meridional section in the trigonometric series (17) in each approximation:

$$\sum_{q=1}^{M} (B_{zp}^{zi(q)} \overline{u}_{zp} + B_{rp}^{zi(q)} \overline{u}_{rp} + B_{\varphi p}^{zi(q)} \overline{u}_{\varphi p}) = D_{zi},$$

$$\sum_{q=1}^{M} (B_{zp}^{ri(q)} \overline{u}_{zp} + B_{rp}^{ri(q)} \overline{u}_{rp} + B_{\varphi p}^{ri(q)} \overline{u}_{\varphi p}) = D_{ri},$$

$$\sum_{q=1}^{M} (B_{zp}^{\varphi i(q)} \overline{u}_{zp} + B_{rp}^{\varphi i(q)} \overline{u}_{rp} + B_{\varphi p}^{\varphi i(q)} \overline{u}_{\varphi p}) = D_{\varphi i}$$

$$(p = i, j, k), \quad \langle i = 1, 2, \ldots, N \rangle. \tag{20}$$

The number of these systems is equal to the number of terms kept in the solution. The matrix elements of these systems are calculated from the coefficients of the constitutive equations and the coordinates of the element vertices in the meridional plane, while the right-hand side of the system is calculated from the amplitudes of the additional stresses σ_{ij}^*, and the volume and surface loads at the appropriate points of the meridional section.

The expressions for the coefficients appearing in (18)–(20) are presented in [3, 6, 19, etc.].

The coefficients $\overline{\overline{T}}_m$ and $\overline{\overline{u}}_i^{(m)}$ are defined by similar expressions, where m should be replaced by $-m$ and all quantities with overbar by quantities with double overbar and vice versa.

If the values of $\overline{T}_m$, $\vec{\overline{T}}_m$ and $\overline{u}_i^{(m)}$, $\overline{\overline{u}}_i^{(m)}$ are known at all points of the finite-element partition of the meridional section, the temperature and displacement components in the body can be found by calculating the trigonometric series (16), (17). Next, the strain and stress components are calculated in each approximation at the current instant. The number of necessary approximations is determined from the condition that the relative change in the SSS in two successive solutions is less than a given value.

2. Numerical Results. To evaluate the influence of various approaches to the plotting of the diagram of material behavior under unloading, we will study the SSS of a thick-walled cylinder [15] with half the meridional section shown in Fig. 1. Its end $z = 0$ is hinged ($t_{nr} = 0, w = 0$) and heat-insulated ($\partial T / \partial z = 0$). At the initial instant, the cylinder is at $T = 293$ K and in stress-free state. The process loading and heating includes two stages. At the first stage, the part of the surface ABC is subject to convective heat exchange with the environment of temperature θ_1. The heat transfer factor α varies linearly from $\alpha = 1.0$ W/(cm^{2}K) at the point B to $\alpha = 0$ at the points A and C. The other part of the cylinder is heat-insulated. At the second stage, the cylinder is cooled (the environment temperature is much lower than the initial temperature at the same values of the heat-transfer factor on the surfaces), while the load $t_{nz} = -5$ MPa is applied to a part of the end surface.

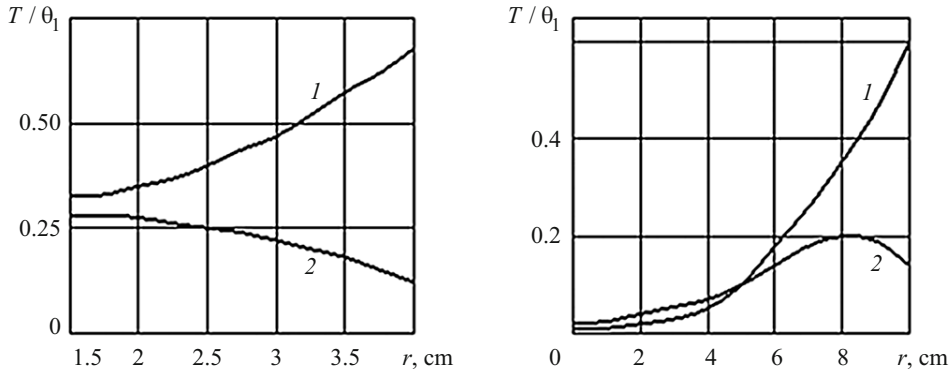

a *b*

Fig. 2

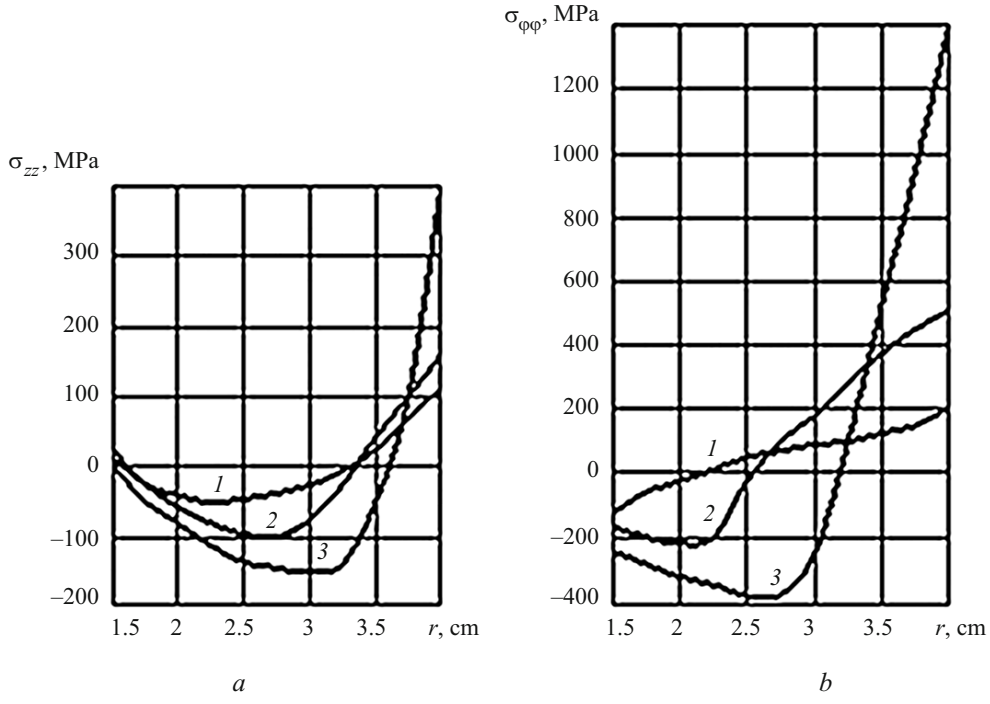

a *b*

Fig. 3

Figure 2 illustrates how the relative temperature T / θ_1 varies along the cylinder radius at $z = 9.25$ cm (Fig. 2*a*) and along the cylinder length at $r = 3.25$ cm (Fig. 2*b*). It can be seen that heating of the cylinder induces high temperature gradients in the radial and axial directions (curves *1*). The analysis of the cylinder SSS calculated with allowance for the perfect Bauschinger effect under unloading shows that the nonuniform heating at the first stage leads to the development of plastic strains in the major part of the cylinder volume (dashed in Fig. 1). At the second stage, cooling and application of a tensile axial load to a part of the end give rise to a zone where unloading and secondary plastic strains occur (hatched in Fig. 1; second stage in Fig. 2, curves *2*).

Let us analyze the stress state of the cylinder in the section $z = 9.25$ cm under different assumptions on the material behavior under unloading. The calculated results corresponding to completion of the second stage of loading are shown in Fig. 3 which illustrates how the axial σ_{zz} (Fig. 3*a*) and circumferential $\sigma_{\varphi\varphi}$ (Fig. 3*b*) stresses vary in the radial direction. Curves *1* represent the perfect Bauschinger effect (15); curves *2*, isotropic hardening (14); and curves *3*, elastic unloading (13) without secondary plastic strains. Comparing these curves shows that allowing for the secondary plastic strains results in substantial redistribution of the stress components, which leads to a considerable decrease in the maximum tensile axial, σ_{zz}, and circumferential, $\sigma_{\varphi\varphi}$, stresses near the outside surface of the cylinder.

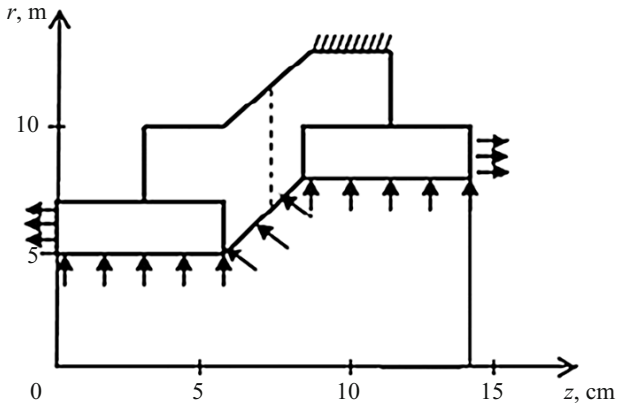

Fig. 4

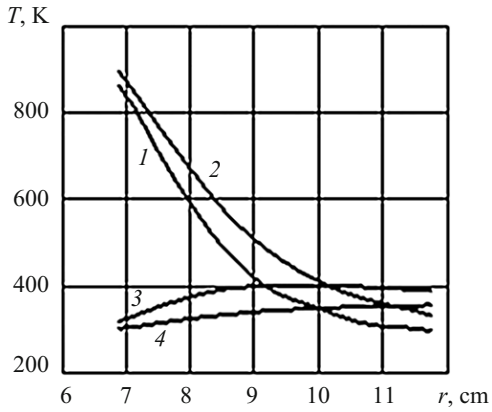

Fig. 5

From the above results it also follows that the maximum stresses decrease in going over from unloading without secondary plastic strains to isotropic hardening. The minimum level is observed for the perfect Bauschiner effect. The secondary plastic strains increase in the same order. Since [9] the true unloading diagram under repeated loading lies between the curves corresponding to isotropic hardening and perfect Bauschiner effect, the calculations of the SSS of the structural member determine the range covering the stress values corresponding to real diagrams.

Let us consider, as an example, the thermostress state of a body of revolution with half the meridional section and loading scheme shown in Fig. 4. The body consists of two cylinders made of EI-437 alloy connected by a sleeve made of EI-395 alloy. The necessary input data are borrowed from [1, 5].

This structural member is subject to the following thermal and mechanical loading. During the first 60 sec, the inside surface is heated by the environment of temperature $\theta = 973$ K, the heat transfer factor being $\alpha = 0.5$ W/(cm^{2}K). This surface is acted upon by pressure P = 10 MPa, the left and right ends are subjected to distributed load $t_{nz} = -10.42$ and 17.78 MPa, respectively. From the 60th second to the 300th second, the body is cooled ($\alpha = 293$ K, $\alpha = 0.3$ W/(cm^{2}K)) without mechanical load. The body is fixed over a part of the outside surface, where the displacement components are set zero. The other parts of the surface are not loaded and heated/cooled.

To plot the diagram of variable deformation, we assumed that the materials of the structural member demonstrate the perfect Bauschinger effect. The whole process was divided into stages by instants 5, 30, 45, 60, 65, 90, 120, 300 sec, and the heat-conduction problem was solved using both explicit and implicit difference schemes. The explicit difference scheme was used until the instant t = 65 sec. After that, the implicit scheme was used.

The results obtained are presented in Figs. 5–7.

Figure 5 shows tje distribution of the temperature along the radius in the section shown in Fig. 4 at $z = 0.0788$ m during heating (curve *1* at $t = 30$ sec, curve *2* at $t = 60$sec) and cooling (curve *3* at $t = 120$ sec, curve *4* at $t = 300$ sec). These figures allow estimating the change in the temperature gradient during heating and cooling.

The development of the zones of inelastic deformation during heating and cooling for t = 30, 60, 120, and 300 sec is schematized in Fig. 6. The zone of active loading is shown by hataching. The zone where the process direction changes after initial plastic deformation but the inelastic strains remain unchanged, i.e., elastic unloading occurs, is cross-hatched. The part of the meridional section where the secondary plastic strains develop under unloading is shown in black. It can be seen that the major portion of the material undergoes plastic deformation. The plastic zone increases to the end of heating and loading (60th second), and its part changes over into the state of "elastic unloading." During cooling with no mechanical load (to 300th second), a zone occurs where secondary plastic strains develop and the elastic unloading zones enlarge. During cooling, a part of the elastic unloading zone undergoes repeated plastic deformation.

Figure 7 illustrates the variation in the axial, σ_{zz} (Fig. 7*a*), and circumferential $\sigma_{\varphi\varphi}$ (Fig. 7*b*), stresses along the radius at $r = 0.0788$ m and different time instants: $t = 30$ sec (curve *1*), $t = 60$ sec (curve *2*), $t = 120$ sec (curve *3*), $t = 300$ sec (curve *4*). As is seen, the stresses remain high to the completion of cooling despite the fact that the mechanical load is absent and the gradients and temperature are low. This is because a considerable plastic strain causing high residual stresses was accumulated to the

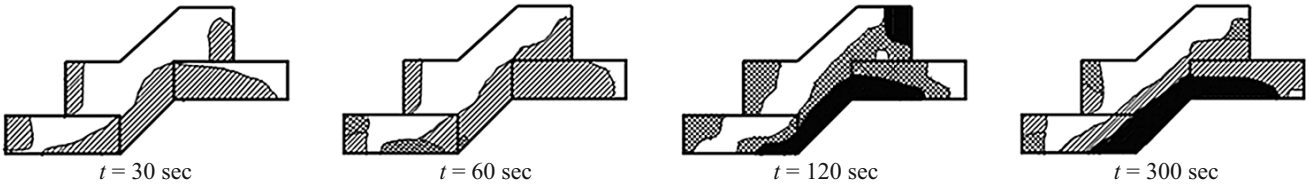

Fig. 6

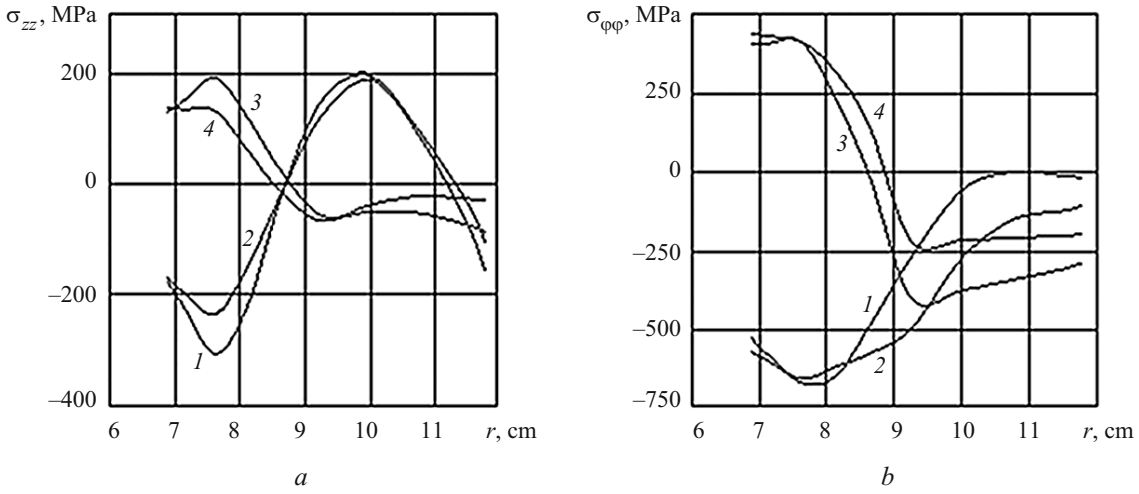

Fig. 7

instant of change in the direction of the process. This fact clearly indicates the necessity of allowing for the loading history in studying the stress state in structural members under variable loading that causes plastic strains.

Conclusions. We have proposed a technique for studying the nonaxisymmetric thermostress state of axisymmetric bodies under combined nonisothermal loading, allowing for the occurrence of plastic strains with opposite sign to the original strains. If the experimental diagrams of loading, unloading, and repeated loading by the load of opposite sign are absent, the stress state of the structural member is determined making some assumptions on material behavior under unloading such as elastic unloading, isotropic hardening, or perfect Bauschiger effect. Using a specific example, we have illustrated how the results obtained depend on the model chosen to describe the material behavior under unloading. Calculations based on the the two last models define the range into which the true values of the stresses fall.

REFERENCES

1. N. I. Bezukhov, V. L. Bazhanov, I. I. Gol'denblat, et al., *Design for Strength*, *Stability*, *and Vibrations at High Temperatures* [in Russian], Mashinostroenie, Moscow (1965).
2. I. A. Birger, B. F. Shorr, I. V. Dem'yanushko, et al., *Thermal Strength of Machine Parts* [in Russian], Mashinostroenie, Moscow (1975).
3. Ya. M. Grigorenko, Yu. N. Shevchenko, et al., *Numerical Methods*, Vol. 11 of the 12-volume series *Composite Mechanics* [in Russian], "A.S.K", Kyiv (2002).
4. Yu. N. Shevchenko, M. E. Babeshko, V. V. Piskun, and V. G. Savchenko, *Spatial Thermoplasticity Problems* [in Russian], Naukova Dumka, Kyiv (1980).
5. Yu. N. Shevchenko, M. E. Babeshko, and R. G. Terekhov, *Thermoviscoplastic Processes of Combined Deformation of Structural Members* [in Russian], Naukova Dumka, Kyiv (1992).
6. Yu. N. Shevchenko and V. G. Savchenko, *Thermoviscoplasticity*, Vol. 2 of the five-volume series *Mechanics of Coupled Fields in Structural Members* [in Russian], Naukova Dumka, Kyiv (1987).

7. Yu. N. Shevchenko, V. G. Savchenko, and D. A. Ishchenko, *Method and Software for Analysis of the Nonstationary Heat Conduction in and the Elastoplastic Stress–Strain State of Structural Members such as Solids of Revolution under Axisymmetric Mechanical and Thermal Loads* [in Russian], Guidelines, Inst. Mekh. AN USSR, Kyiv (1988).
8. Yu. N. Shevchenko, V. G. Savchenko, D. A. Ishchenko, and V. M. Pavlychko, *Method and Applied Software for Analysis of the Nonstationary Heat Conduction in and the Elastoplastic Stress–Strain State of Structural Members such as Solids of Revolution under Axisymmetric Mechanical and Thermal Loads* [in Russian], Recommendations R 54-284-90, VNIINMASh, Moscow (1990).
9. M. E. Babeshko and V. G. Savchenko, "Axisymmetric elastoplastic state of compound shells subject to thermal and mechanical loading and radiation exposure," *Int. Appl. Mech.*, **53**, No. 4, 368–373 (2017).
10. M. E. Babeshko and V. G. Savchenko, "Analyzing processes of nonisothermal loading of shells of revolution with allowance for repeated plastic strains," *Int. Appl. Mech.*, **53**, No. 6, 639–646 (2017).
11. M. E. Babeshko and V. G. Savchenko, "On allowance for the third invariant of stress deviator in analysis of processes of deformation of thin shells," *Int. Appl. Mech.*, **54**, No. 2, 163–171 (2018).
12. M. E. Babeshko and V. K. Stryuk, "Calculating the stress state of a solid cylinder on the basis of the theory of flow with isotropic hardening," *Sov. Appl. Mech.*, **10**, No. 6, 587–591 (1974).
13. V. A. Bazhenov, M. O. Vabishchevich, I. I. Solodei, and E. A. Chepurnaya, "Semianalytic finite-element method in dynamic problems of linear fracture mechanics," *Int. Appl. Mech.*, **54**, No. 5, 519–530 (2018).
14. H. Hencky, "Zur theorie der plastischer deformationen und der hierdurch im material hervorgerufenen nachspannungen," *ZAMM*, **4**, No. 4, 323–334 (1924).
15. D. A. Ishchenko and V. G. Savchenko, "Influence of taking account of secondary plastic deformations on the solution of the axisymmetric thermoplasticty problem," *Sov. Appl. Mech.*, **24**, No. 3, 229–233 (1988).
16. L. Prandtl, "Anwendungsbeispile zu einem Henckyschen satz uber das platische gleichgewicht," *ZAMM*, **3**, No. 6, 401–406 (1923).
17. A. Reuss, "Berucksichtigung der elastischen formanderung in der plastizitatstheorie," *ZAMM*, **10**, No. 3, 266–274 (1930).
18. V. G. Savchenko and M. E. Babeshko, "Thermostressed state of layered bodies of revolution damaging under deformation," *Int. Appl. Mech.*, **54**, No. 3, 287–305 (2018).
19. Yu. N. Shevchenko and V. G. Savchenko, "Three-dimensional problems of thremoviscoplasticity: focus on Ukrainian research (Review)," *Int. Appl. Mech.*, **52**, No. 3, 217–271 (2016).
20. E. A. Storozhuk, I. S. Chernyshenko, and O. V. Pigol', "Elastoplastic state of an elliptical cylindrical shell with a circular hole," *Int. Appl. Mech.*, **53**, No. 6, 647–654 (2017).
21. M. Zyczkowskii, *Combined Loadings in the Theory of Plasticity*, PWN, Polish Scientific Publishers, Warsaw (1981).